HEFAT2014
10th International Conference on Heat Transfer, Fluid Mechanics and Thermodynamics
14 – 16 July 2014
Orlando, Florida

MULTI-PARAMETER OPTIMIZATION OF A PLANE FIN HEAT SINK WITH ELLIPTIC SHAPED SURFACE SCALES

George DeMoulin* and Ivan Catton.
*Author for correspondence
Department of Mechanical and Aerospace Engineering,
University of California Los Angeles,
Los Angeles, CA,
USA,
E-mail: gdemoulin@ucla.edu

ABSTRACT

With the increase in power consumption within a limited volume of present day power electronics, heat sink design has become a central aspect of thermal management of these devices. In this study, a plane fin heat sink with surface augmentation was optimized to meet and exceed the operating requirements of DARPA's Microtechnologies for Air Cooled Exchangers (MACE) program. To accomplish the computational efficiency required of a multi-parameter optimization problem, conjugate heat transfer and fully developed flow were modeled using Volume Averaging Theory (VAT). By modeling a highly detailed heterogeneous structure as a homogeneous porous medium, VAT based numerical simulation overcomes the meshing difficulties and computational cost associated with traditional CFD methods. The configuration considered was elliptic scales located on the fin surfaces where the scale height, transverse pitch, and longitudinal pitch were variable. These parameters along with fin base thickness, tip thickness, and fin pitch were varied simultaneously while the heat sink length (101.6mm), width (101.6mm), and height (25.4mm) were held constant. Design of Experiments (DOE) software was used to conduct a Response Surface Methodology (RSM) design to minimize the thermal resistance with constant pumping power as the flow condition. The optimized heat sink presented has a thermal resistance of 0.0246°C/W when cooled by air with a pumping power of 33W.

INTRODUCTION

Preventing semiconductor failure while minimizing the size and power input for air moving devices has been a challenge for researchers over the past few decades. Many innovative concepts for air cooled heat sinks [1-4] and liquid cooled microchannel heat sinks [5-7] continue to be developed in efforts to achieve highly efficient electronic cooling systems. However, much of the design over the years has been empirical in nature. A more systematic approach to designing advanced heat sinks is multi-parameter optimization. The key challenge present in all optimization techniques is acquiring an accurate yet efficient simulation model. CFD simulations including conjugate effects are highly accurate, and have been used to optimized heat sinks [8,9], but the computational cost associated with these simulations limits the optimization capability. An approach to modeling conjugate heat transfer that is very suitable for heat sink optimization is Volume Averaging Theory (VAT).

Volume Averaging Theory (VAT), first developed in the 1960s, has been shown to be a powerful tool for modeling conjugate heat transfer in heat sinks and heat exchangers. This modeling technique treats a heterogeneous system with two phases (solid and fluid) as a homogeneous porous medium. The development of the VAT governing equations begins by applying rigorous averaging procedures to a Representative Elementary Volume (REV) within the macroscopic system. The resulting set of differential equations, while simplified, requires closure of integral terms that appear as a result of the averaging process. The closure of these terms is accomplished using friction factor and Nusselt number correlations, which can be obtained for a wide variety of geometric configurations. Closure expressions can also be obtained for heat sinks with surface augmentation [10]. The configuration used in this study is elliptic shaped scales located on the surfaces of a plane fin heat sink, as shown in Figure 1a. The computational domain and coordinate system for the VAT based numerical simulation is shown in Figure 1b.

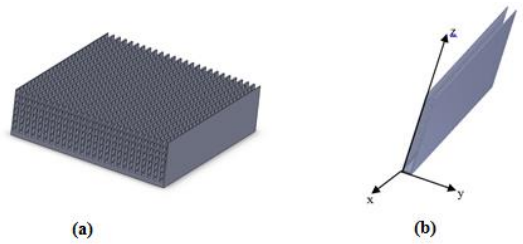

Figure 1 (a) Plane fin heat sink with elliptic surface scales and (b) computational domain and coordinate system.

The closed set of VAT based governing equations can then be solved numerically without the need to create a highly detailed mesh. Most VAT based simulations for heat sinks run in less than one minute on a PC. The geometric parameters of a heat sink can then be optimized using techniques such as Design of Experiments (DOE). The type of DOE design used in this work is based on Response Surface Methodology (RSM), where one response variable is minimized while varying multiple parameters simultaneously. Because DOE is a very systematic approach to optimization, in many cases it requires fewer simulations than other methods such as Genetic Algorithm (GA) or Particle Swarm Optimization (PSO).

NOMENCLATURE

A,B,C	[s^{-1}]	Finite difference matrices
A_w	[m^2]	Wetted surface area
b	[-]	Empirical coefficient
C_μ	[-]	Empirical coefficient
c_p	[J/kg-K]	Specific heat
D_h	[m]	Hydraulic diameter
e	[m]	Scale height
F	[m]	Finite difference matrix
F_p	[m]	Fin pitch
f_f	[-]	Friction factor
h	[m]	Grid spacing
H	[m]	Fin height
k	[W/m-K]	Thermal conductivity
l	[m]	Turbulent mixing length
$<m>$	[-]	Porosity
p	[Pa]	Pressure
Pr	[-]	Prandtl number
Q	[W]	Heat transfer rate
Re	[-]	Reynolds number
S_w	[m^{-1}]	Specific surface area
$\tilde{\bar{u}}$	[m/s]	Volume average velocity
$\tilde{\bar{T}}$	[K]	Volume average temperature

Special Characters

α	[W/m^2-K]	Heat transfer coefficient
ρ	[kg/m^3]	Density
v	[m^2/s]	Kinematic viscosity
$\Delta\Omega$	[m^3]	Volume of REV

Subscripts and Superscripts

f	Fluid phase
S	Solid phase
T	Temperature or turbulent

VAT BASED GOVERNING EQUATIONS

Volume Averaging Theory (VAT), first developed by Whitaker [11], is a rigorous mathematical procedure where point-wise correct conservation equations are averaged over a Representative Elementary Volume (REV). The resulting equation set represents the system in a hierarchical manner, which makes VAT an effective tool for studying the system effects of various parameters. Because quantities such as velocity, pressure, and temperature are averaged over a large scale volume, VAT based numerical simulations run much faster than time consuming CFD simulations. Equation 1 shows the VAT based continuity equation for incompressible flow.

$$\frac{\partial \tilde{\bar{u}}}{\partial x}+\frac{\partial \tilde{\bar{v}}}{\partial y}=0 \tag{1}$$

The volume averaged momentum conservation equation for fully developed turbulent flow is:

$$0=-\frac{1}{\rho_f}\frac{d\langle \bar{p}\rangle_f}{dx}+f_f\frac{S_w}{\langle m(z)\rangle}\frac{\tilde{\bar{u}}^2}{2} +\frac{\partial}{\partial z}\left(\langle m(z)\rangle(\nu+\nu_T)\frac{\partial \tilde{\bar{u}}}{\partial z}\right) \tag{2}$$

The last term on the right hand side of Equation 2 is closed using the turbulent kinetic energy equation of Gratton et al. [12],

$$\tilde{\nu}_T\left(\frac{\partial \tilde{\bar{u}}}{\partial x}\right)^2+\frac{\partial}{\partial x}\left[\left(\frac{\tilde{\nu}_T}{\mathrm{Pr}_T}+\frac{1}{\mathrm{Re}_{por}}\right)\frac{\partial b}{\partial x}\right]+\frac{f_f\tilde{\bar{u}}^3}{\langle m(z)\rangle} +\frac{2}{\mathrm{Re}_{por}}\left(\frac{\partial\sqrt{b}}{\partial x}\right)^2=C_\mu\frac{b^2}{\tilde{\nu}_T} \tag{3}$$

The turbulent kinetic energy $\tilde{\nu}_T$ is expressed in terms of a mixing length, $l(z)$, defined by Travkin and Catton [13].

$$\tilde{\nu}_T=C_\mu l(z)\sqrt{b} \tag{4}$$

The volume averaged equation for conservation of energy in the fluid phase is given by:

$$c_{pf}\rho_f\langle m(z)\rangle\tilde{\bar{u}}\frac{\partial \tilde{\bar{T}}_f}{\partial x}=\frac{\partial}{\partial z}\left(\langle m(z)\rangle\left(\tilde{k}_T+k_f\right)\frac{\partial \tilde{\bar{T}}_f}{\partial z}\right) +\tilde{\alpha}_T S_w\left(\tilde{\bar{T}}_s-\tilde{\bar{T}}_f\right) \tag{5}$$

And the energy equation for the solid phase is:

$$0 = \frac{\partial}{\partial x}\left(\left(1-\langle m(z)\rangle\right)k_{ST}\frac{\partial \tilde{\bar{T}}_s}{\partial x}\right) + \frac{\partial}{\partial z}\left(\left(\left(1-\langle m(z)\rangle\right)k_{ST}\frac{\partial \tilde{\bar{T}}_s}{\partial z}\right)\right) - \tilde{\alpha}_T\, S_w\left(\tilde{\bar{T}}_s - \tilde{\bar{T}}_f\right) \quad (6)$$

The VAT based momentum and energy equations shown here need expressions for $\langle m(z)\rangle$, S_w, f_f, and $\tilde{\alpha}_T$ to obtain closure. The porosity $\langle m(z)\rangle$ and the specific surface area S_w are functions of geometry only and are easily determined. The internal friction factor f_f and heat transfer coefficient $\tilde{\alpha}_T$ can be determined either by experiment or CFD. Using CFD, Zhou et al. [10] provides the following expressions to close the VAT equation set for plane fin heat sinks with elliptic surface scales. The porosity and specific surface area are determined from Equations 7 and 8.

$$\langle m\rangle = 1 - \frac{\Delta\Omega_S}{\Delta\Omega} = \frac{H - 2\kappa e}{F_p} \quad (7)$$

$$S_w = \frac{A_w}{\Delta\Omega} = \frac{2P_tP_l + \pi\left[\frac{3}{4}\left(P_t+P_l\right) - \frac{1}{2}\sqrt{P_tP_l}\right]e}{P_tP_lF_p} \quad (8)$$

$$f_f = \left[\frac{94.53}{\mathrm{Re}_{D_h}} + 0.0019\,\mathrm{Re}_{D_h}^{0.217} + 3.544\left(\frac{e}{D_h}\right)^{1.465}\left(\frac{H}{D_h}\right)^{0.0232}\right]\left(\frac{P_t}{P_l}\right)^{S_2} \quad (9)$$

where

$$S_2 = \left(-\frac{129.28}{\mathrm{Re}_{D_h}} + 2.74\right)\left(\frac{e}{D_h}\right)^{0.771} \quad (10)$$

$$Nu^* = \left\{0.144\,\mathrm{Re}_{D_h}^{0.765}\left[\left(\frac{e}{D_h}\right)^{0.695} + 0.457\right]\left(\frac{H}{D_h}\right)^{1.018} + 8.235\right\}\left(\frac{P_t}{P_l}\right)^{S_1} \quad (11)$$

where

$$S_1 = \left(\frac{e}{D_h}\right)^{0.539} \quad (12)$$

Where the hydraulic diameter is given by:

$$D_h = \frac{4\langle m\rangle}{S_w} \quad (13)$$

The hydrodynamic boundary conditions used in this analysis are no-slip surfaces at the top and bottom walls. In the optimization study a constant temperature boundary condition was used at the base to achieve the fastest running simulations. After the optimized configuration was obtained a constant heat input of 1000W was used to verify that the heat sink met DARPA's MACE program goals. For all cases the thermal boundary condition at the top surface was adiabatic.

NUMERICAL SOLUTION OF GOVERNING EQUATIONS

The VAT momentum and energy conservation equations are solved using finite difference numerical methods. The computational domain is discretized using a Cartesian grid, 50 by 100 points, refined near the lower boundary. The finite difference approximations in the governing equations are based on a three point grid stencil. Three point central differencing is applied to interior grid points, and two point one-sided differencing is applied at all boundaries. Equations 14-20 show the discretized VAT momentum conservation equation.

$$A_{ju}^s u_{j-1}^{s+1} - C_{ju}^s u_j^{s+1} + B_{ju}^s u_{j+1}^{s+1} = -F_{ju}^s \quad (14)$$

where

$$A_{ju}^s = \frac{a_j^s}{h_j\bar{h}_j} \quad (15)$$

$$B_{ju}^s = \frac{a_{j+1}^s}{h_{j+1}\bar{h}_j} \quad (16)$$

$$C_{ju}^s = \frac{a_j^s}{h_j\bar{h}_j} + \frac{a_{j+1}^s}{h_{j+1}\bar{h}_j} + \frac{1}{2}c_{dj}S_{wj}\tilde{\bar{u}}^s \quad (17)$$

$$F_{ju}^s = -\frac{\langle m\rangle_j}{\rho_f}\left(\frac{d\tilde{p}}{dx}\right)^s \quad (18)$$

$$\bar{h}_j = \frac{h_j + h_{j+1}}{2} \quad (19)$$

$$a_j = \frac{1}{2}\left[\langle m\rangle_j\left(\nu_T^s + \nu\right)_j + \langle m\rangle_{j-1}\left(\nu_T^s + \nu\right)_{j-1}\right] \quad (20)$$

The superscript $s+1$ denotes the updated value of u. Iterations are performed on Equation 14 until sufficient

convergence is obtained. The energy equations for the solid and fluid phases in 2-D are discretized in a similar manner. The discretization of the fluid phase energy equation is shown in Equations 21-26.

$$A^s_{jTF}\tilde{\bar{T}}^s_{i,j-1} - C^s_{jTF}\tilde{\bar{T}}^s_{i,j} + B^s_{jTF}\tilde{\bar{T}}^s_{i,j+1} + C^s_{jTF}\tilde{\bar{T}}^s_{S_{i,j}} = -F^s_{iTF} \quad (21)$$

where

$$A^s_{jT} = \frac{a^s_j}{h_j\bar{h}_j} \quad (22)$$

$$B^s_{jT} = \frac{a^s_j}{h_j\bar{h}_j} \quad (23)$$

$$C^s_{jT} = \frac{a^s_j}{h_j\bar{h}_j} + \frac{a^s_{j+1}}{h_{j+1}\bar{h}_j} + \frac{1}{h_i}\left(c_p\rho_f\langle m\rangle\tilde{\bar{u}}\right)^s_j + \tilde{\alpha}_{Tj}S_{wj} \quad (24)$$

$$F^s_{jT} = \left(c_{pf}\rho_f\langle m\rangle\tilde{\bar{u}}\right)_j\frac{\tilde{\bar{T}}^s_{i-1,j}}{h_i} \quad (25)$$

$$a_j = \frac{1}{2}\left[\langle m\rangle_j\left(k^s_T + k_f\right)_j + \langle m\rangle_{j-1}\left(k^s_T + k_f\right)_{j-1}\right] \quad (26)$$

Similarly, the finite difference equations for the solid phase are:

$$A^s_{jTS}\tilde{\bar{T}}^s_{i,j-1} - C^s_{jTS}\tilde{\bar{T}}^s_{i,j} + B^s_{jTS}\tilde{\bar{T}}^s_{i,j+1} + C^s_{jTS}\tilde{\bar{T}}^s_{S_{i,j}} = -F^s_{iTS} \quad (27)$$

where

$$A^s_{jT} = \frac{a^s_j}{h_j\bar{h}_j} \quad (28)$$

$$B^s_{jTS} = \frac{a^s_j}{h_j\bar{h}_j} \quad (29)$$

$$C^s_{jT} = \frac{a^s_j}{h_j\bar{h}_j} + \frac{a^s_{j+1}}{h_{j+1}\bar{h}_j} + \frac{a^s_j}{h_i\bar{h}_i} + \frac{a^s_j}{h_{i+1}\bar{h}_{i+1}} + \tilde{\alpha}_{Tj}S_{wj} \quad (30)$$

$$F^s_{jTS} = -\left(\frac{a_j}{h_j\bar{h}_j}\right)T^s_{S_{i,j-1}} - \left(\frac{a_{j+1}}{h_{j+1}\bar{h}_j}\right)T^s_{S_{i,j}} \quad (31)$$

$$a_j = \frac{1}{2}\left[\left(1-\langle m\rangle_j\right)k^s_{sj} + \left(1-\langle m\rangle_{j-1}\right)k^s_{sj-1}\right] \quad (32)$$

The VAT fluid and solid energy conservation equations are solved using and Alternating Direction Implicit (ADI) method. In a two-dimensional case the ADI scheme sweeps through the computational grid in one direction to obtain intermediate values, s+1/2, and uses these values as it sweeps through the grid in the second direction to obtain the updated values s+1. For the fluid energy equation, the first sweep is in the z-direction

$$A^s_{jTF}\tilde{\bar{T}}^{s+1/2}_{i,j-1} + B^s_{jTF}\tilde{\bar{T}}^{s+1/2}_{i,j} + C^s_{jTF}\tilde{\bar{T}}^{s+1/2}_{i,j+1} + D^s\tilde{\bar{T}}^{s+1/2}_{S_{i,j}} = F^s_{iTF} \quad (33)$$

The updated values, $\tilde{\bar{T}}_{s+1}$, are then determined by sweeping through the grid in the x-direction.

$$A^s_{iTF}\tilde{\bar{T}}^{s+1}_{i-1,j} + B^s_{iTF}\tilde{\bar{T}}^{s+1}_{i,j} + C^s_{iTF}\tilde{\bar{T}}^{s+1}_{i+1,j} + D^s\tilde{\bar{T}}^{s+1}_{S_{i,j}} = F^{s+1/2}_{jTF} \quad (34)$$

Similarly, the ADI equation for the solid energy equation in the z-direction is:

$$A^s_{jTS}\tilde{\bar{T}}^{s+1/2}_{S_{i,j-1}} + B^s_{jTS}\tilde{\bar{T}}^{s+1/2}_{S_{i,j}} + C^s_{jTS}\tilde{\bar{T}}^{s+1/2}_{S_{i,j+1}} + D^s\tilde{\bar{T}}^{s+1/2}_{i,j} = F^s_{iTS} \quad (35)$$

And for the x-direction,

$$A^s_{iTS}\tilde{\bar{T}}^{s+1}_{S_{i-1,j}} + B^s_{iTS}\tilde{\bar{T}}^{s+1}_{S_{i,j}} + C^s_{iTS}\tilde{\bar{T}}^{s+1}_{S_{i+1,j}} + D^s\tilde{\bar{T}}^{s+1}_{i,j} = F^{s+1/2}_{jTS} \quad (36)$$

A flow chart illustrating the entire solution process is shown in Figure 2.

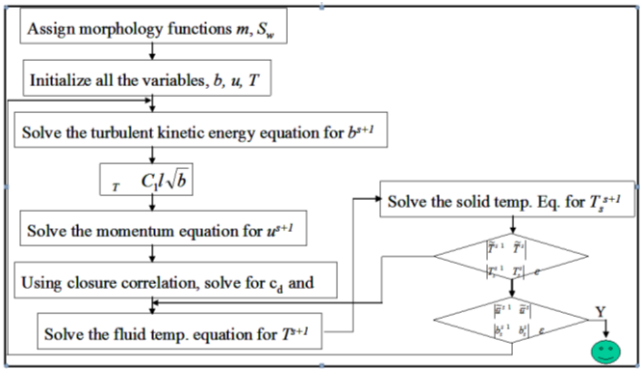

Figure 2 Numerical solution method flow chart

OPTIMIZATION BY DESIGN OF EXPERIMENTS

The geometric parameters of a plane fin heat sink with elliptic surface scales were optimized while maintaining a constant pumping power of 33W. All simulations were for aluminum heat sinks cooled by air at 15°C. A DOE optimization study based Response Surface Methodology (RSM) was used to minimize the quantity $1/Q_{tot}$ where Q_{tot} is the total heat input at

the baseplate of the heat sink. Table 1 shows the dimensions of the parameters that were held constant and the ranges for the six parameters that were varied.

Table 1 Dimensions and ranges for optimization of elliptic scale heat sink

Parameter	Value/ Range
Heat sink width (mm)	101.6
Heat sink length (mm)	101.6
Fin height (mm)	25.4
Baseplate thickness (mm)	1
Fin thickness at base, WRH (mm)	1-3
Fin thickness at tip, WRHT (mm)	0.5-2
Pitch/fin thickness ratio at base, POY	1.5-3
Surface scale height, ESC (mm)	0.05-0.1
Surface scale transverse pitch, PT (mm)	1-4
Surface scale transverse/longitudinal pitch, PTOL	0.5-2.5

The response surface resulting from the DOE optimization in Figure 3 shows the response variable $1/Q_{tot}$ as a function of the parameters POY and PTOL. Although the response surface represents a saddle point solution, only one of the six parameters was found to be optimal at the lower bound. The optimal dimensions predicted by the response surface are shown above the name of the variable in Figure 2. The units of WRH, WRHT, ESC, and PT are millimeters.

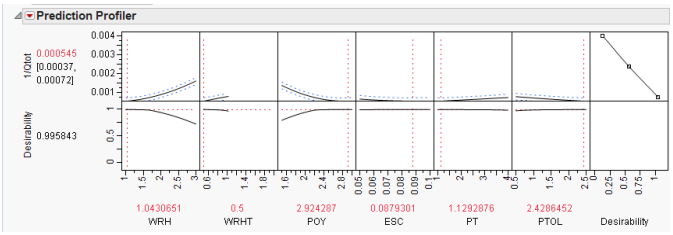

Figure 2 Prediction profiler displaying optimum parameters.

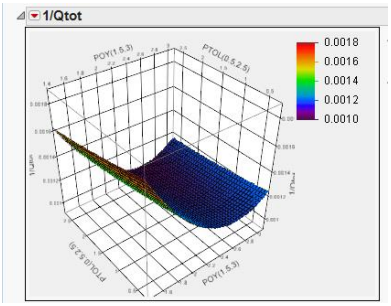

Figure 3 Response surface of ($1/Q_{tot}$) versus dimensionless fin pitch and dimensionless scale transverse pitch.

The dimensions of the optimized elliptic scale heat sink are shown in Table 2. The maximum midpoint temperature of the optimized heat sink is 37.3°C, which is well below the target temperature of 65°C. The thermal resistance is 0.0246°C/W and the heat sink mass is 222g.

Table 2 Dimensions of optimized elliptic scale heat sink

Parameter	Value
Heat sink width (mm)	101.6
Heat sink length (mm)	101.6
Fin height (mm)	25.4
Baseplate thickness (mm)	1
Fin thickness at base, WRH (mm)	1.04
Fin thickness at tip, WRHT (mm)	0.5
Pitch/fin thickness at base, POY (mm)	2.92
Fin Pitch (mm)	3.04
Surface scale height, ESC (mm)	0.0879
Scale transverse pitch, PT (mm)	3.65
Scale transverse/longitudinal pitch, PTOL	2.43
Scale longitudinal pitch, PL (mm)	1.50
Pumping power (W)	33
Midpoint baseplate temperature (°C)	39.6
Thermal Resistance (°C/W)	0.0246
Heat sink mass (g)	222

CONCLUSIONS

Design of Experiments aided by VAT based numerical simulation has been shown to be a very effective approach to heat sink optimization. A plane fin heat sink with elliptic scale-roughened surfaces was successfully optimized and found to exceed all of DARPA's MACE program goals. With a total heat input of 1000W and 33W pumping power, the optimized heat sink had a thermal resistance of 0.0246 °C/W and a maximum midpoint temperature of 39.6°C. The findings of this work demonstrate that modeling conjugate heat transfer using Volume Averaging Theory opens the door to optimizing heat sinks with enhanced surfaces.

ACKNOWLEDGEMENTS

The support of a DARPA initiated grant within the MACE program, Grant No. W31P4Q-09-1-0005, is gratefully acknowledged. The views, opinions, and/or findings contained in this article are those of the author and should not be interpreted as representing the official views or policies, either expressed or implied, of the Defense Advanced Research Projects Agency or the Department of Defense.

REFERENCES

[1] Allison, J. M., Staats, W. L., McCarthy, M., Jenicek, D., Edoh, A. K., Lang, J. H., and Brisson, J. G., 2011,"Enhancement of convective heat transfer in an air-cooled heat exchanger using interdigitated impeller blades," International Journal of Heat and Mass Transfer, 54(21), pp.4549-4559.

[2] Wu, W., Bostanci, H., Saarloos, B.A., Du, J.H., Lin, Y.R., Rini, D.P, and Chow, L.C., 2011,"Evaluation of compact and effective air-cooled carbon foam heat sink," Journal of Heat Transfer, 133(5), 054504-2.

[3] Yu, Y., Simon, T. W., Zhang, M., Yeom, T., North, M. T., & Cui, T., 2014, "Enhancing heat transfer in air-cooled heat sinks using piezoelectrically-driven agitators and synthetic jets," International Journal of Heat and Mass Transfer, 68, 184-193.

[4] Yu, Y., Simon, T., Agrawal, S., North, M., and Cui, T., 2011, "A Computational Study of Active Heat Transfer Enhancement of Air-Cooled Heat Sinks by Actuated Plates," ASME 2011 International Mechanical Engineering Congress and Exposition, pp. 885-893.
[5] Xie, G.N., Zhang, F.L., Zhang, W.H, and Sunden, B., 2014, "Constructal Design and Thermal Analysis of Microchannel Heat Sinks with Multistage Bifurcations in Single-phase Liquid Flow," Applied Thermal Engineering, 62, pp.791-802.
[6] Xie, G.N., Chen, Z.Y., Sunden, B., and Zhang, W.H., 2013, "Comparative study of flow and thermal performance of liquid-cooling parallel-flow and counter-flow double-layer wavy microchannel heat sinks," Numerical Heat Transfer, A(64), pp.30-55.
[7] Kalteh, M., Abbassi, A., Saffar-Avval, M., Frijns, A., Darhuber, A., and Harting, J., 2012, "Experimental and numerical investigation of nanofluid forced convection inside a wide microchannel heat sink," Applied Thermal Engineering, 36, pp.260-268.
[8] Hung, T.C., and Yan, W.M., 2012, "Optimization of a microchannel heat sink with varying channel heights and widths," Numerical Heat Transfer, A(62), pp. 722-741.
[9] Kanyakam, S., and Bureerat, S., 2012, "Multi-objective optimization of a pin fin heat sink using evolutionary algorithms," Journal of Electronic Packaging, 134, 021008-1.
[10] Zhou, F., & Catton, I. (2013)," A numerical investigation of turbulent flow and heat transfer in rectangular channels with elliptic scale-roughened walls," Journal of Heat Transfer, 135(8), 081901.
[11] Whitaker, S., 1967, "Diffusion and dispersion in porous media," AIChE Journal, 13(3), pp. 420-427.
[12] Travkin, V. S., Catton, I., and Gratton, L., 1993, "Single Phase Turbulent Transport in Prescribed Non-Isotropic and Stochastic Porous Media," ASME -PUBLICATIONS- HTD, 240, p. 43.
[13] Travkin, V. S., and Catton, I., 2001, "Transport phenomena in heterogeneous media based on volume averaging theory," Advances in Heat Transfer, G. G. Hari, and A. H. Charles, eds., Elsevier, pp. 1-144.